ACADEMIC PRESS

Available online at www.sciencedirect.com
SCIENCE DIRECT®

Journal of Catalysis 215 (2003) 344–352

JOURNAL OF CATALYSIS

www.elsevier.com/locate/jcat

Aqueous-phase reforming of methanol and ethylene glycol over alumina-supported platinum catalysts

J.W. Shabaker, R.R. Davda, G.W. Huber, R.D. Cortright, and J.A. Dumesic *

Department of Chemical Engineering, University of Wisconsin, 53706 Madison, WI USA

Received 21 October 2002; revised 17 January 2003; accepted 23 January 2003

Abstract

The rates of aqueous-phase reforming of methanol and ethylene glycol to form H_2 and CO_2 were measured under kinetically controlled reaction conditions at temperatures of 483 and 498 K over alumina-supported platinum catalysts. Results show that the rates of formation of H_2 from aqueous solutions of methanol (from 1 to 10 wt%) are similar to the rates of conversion of ethylene glycol, suggesting that C–C bond cleavage is not rate limiting for ethylene glycol reforming. Aqueous-phase reforming of both oxygenated hydrocarbons over Pt/Al_2O_3 leads to nearly 100% selectivity for the formation of H_2 (compared to the formation of alkanes), suggesting that methanation or Fischer–Tropsch reactions involving CO/CO_2 and H_2 do not appear to be important over platinum-based catalysts under the conditions of the present study. The rate of production of hydrogen is higher order in methanol (0.8) compared to ethylene glycol (0.3–0.5), and the reaction is weakly inhibited by hydrogen (−0.5 order) for both feedstocks. The rates of aqueous-phase reforming of methanol and ethylene glycol show apparent activation barriers of 140 and 100 kJ/mol, respectively, from 483 K and 22.4 bar total pressure to 498 K and 29.3 bar total pressure. Low levels of CO (< 300 ppm) are detected in the gaseous effluents from aqueous-phase reforming of methanol and ethylene glycol over alumina-supported Pt catalysts, suggesting that water–gas shift processes are operative under the aqueous-phase reforming conditions of this study. The observed reaction kinetics for ethylene glycol of this study can be explained by a reaction scheme involving quasi-equilibrated adsorption of ethylene glycol, water, H_2, and CO_2, combined with irreversible steps involving dehydrogenation of adsorbed ethylene glycol to form adsorbed $C_2O_2H_x$* species, cleavage of the C–C bond to form adsorbed COH_y* species, further dehydrogenation leading to adsorbed CO*, and removal of adsorbed CO* by water-gas shift. Aqueous-phase reforming of methanol may take place by a similar reaction scheme, without the step involving cleavage of the C–C bond. The nearly first-order reaction kinetics with respect to methanol can be explained by weaker adsorption of methanol compared to molecular adsorption of ethylene glycol.

Keywords: Methanol; Ethylene glycol; Reforming; Hydrogen production; Supported platinum catalysts

1. Introduction

Fuel cells have emerged as promising devices for clean and efficient generation of power for global energy needs. For example, fuel cells that generate power from hydrogen operate at relatively low temperatures (e.g., 350 K) and produce only water as a by-product. While hydrogen fuel cells have a low impact on the environment, current methods for producing hydrogen require high-temperature steam reforming of nonrenewable hydrocarbon feedstocks. Greater environmental benefits of generating power from hydrogen fuel cells would be realized if the hydrogen fuel could be produced from renewable resources, such as biomass. In particular, H_2 and CO_2 would be produced by reforming of biomass resources, and the CO_2 produced as a by-product would be fixed and stored by plant biomass grown subsequently for further hydrogen production. In this respect, we have recently reported that hydrogen can be produced at relatively low temperatures (e.g., 500 K) over supported Pt catalysts by liquid-phase reforming of biomass-derived oxygenated hydrocarbons (such as methanol, ethylene glycol, glycerol, sorbitol, and glucose) [1]. In addition to utilizing renewable feedstocks, this method of generating hydrogen by liquid-phase reforming of oxygenated hydrocarbons eliminates the need to vaporize water and the oxygenated hydrocarbon (which reduces the energy requirements for producing hydrogen), and the production of H_2 and CO_2 by liquid-phase reforming leads to low levels of CO in a single-step catalytic process.

* Corresponding author.
E-mail address: dumesic@engr.wisc.edu (J.A. Dumesic).

0021-9517/03/$ – see front matter
doi:10.1016/S0021-9517(03)00032-0

Liquid-phase reforming of oxygenated hydrocarbons, such as methanol and ethylene glycol, takes place according to the following stoichiometric reactions:

$$CH_3OH + H_2O \rightarrow 3H_2 + CO_2, \quad (1)$$

$$C_2H_6O_2 + 2H_2O \rightarrow 5H_2 + 2CO_2. \quad (2)$$

These reactions may take place via formation of CO as an intermediate product, which is subsequently converted to CO_2 by the water–gas shift reaction

$$CO + H_2O \leftrightarrow H_2 + CO_2. \quad (3)$$

Alternatively, it is possible that CO_2 could be produced directly. Generation of H_2 and CO_2 by liquid-phase reforming at low temperatures, however, is accompanied by selectivity challenges, since the reaction of H_2 and CO or CO_2 to form alkanes (C_nH_{2n+2}) (e.g., reaction (4) below) and water is also highly favorable at these low temperatures. For example, the equilibrium constant at 500 K for the conversion of CO_2 and H_2 to give methane, by the following reaction, is of the order of 10^{10} per mole of CO_2:

$$CO_2 + 4H_2 \leftrightarrow CH_4 + 2H_2O. \quad (4)$$

In addition, an oxygenated hydrocarbon can form alkanes via cleavage of C–O bonds, followed by hydrogenation, as represented for ethylene glycol by

$$C_2H_6O_2 + 3H_2 \leftrightarrow 2CH_4 + 2H_2O, \quad (5)$$

$$C_2H_6O_2 + 2H_2 \leftrightarrow C_2H_6 + 2H_2O. \quad (6)$$

In the present paper, we report results of experimental studies to determine the intrinsic rates of liquid-phase reforming for methanol and ethylene glycol over alumina-supported platinum catalysts. We conduct reaction kinetics measurements at various temperatures, different concentrations of methanol and ethylene glycol, and different pressures. We use the results from these measurements to suggest the nature of rate-limiting processes for liquid-phase reforming reactions.

2. Experimental

2.1. Catalyst preparation

Alumina-supported catalysts (Catapal B γ-Al_2O_3, Grace) were prepared by incipient wetness impregnation (1.6 cm^3 solution per gram of support) with aqueous solutions of tetraamine platinum nitrate ($Pt(NH_4)_4(NO_3)_2$, Strem Chemicals), followed by treatment in an oven at 373 K for 12 h. All catalysts were subsequently heated to 533 K (1.3 K/min) in a mixture of 10% O_2/He (300 cm^3(STP)/min) in a Pyrex cell and held at 533 K for 2 h. The calcined catalysts were then sieved to a 120–230-mesh size (particle diameters between 63 and 125 μm) and loaded into reactors. Catalyst metal loadings were verified by atomic absorption spectroscopy of the calcined samples (AAS/ICP).

Prior to collection of reaction kinetics data, each catalyst was reduced on the kinetics apparatus in H_2 (100 cm^3 (STP)/min). The reactor was heated to 523 K (0.5 K/min) and then held at this temperature for 2 h. Carbon monoxide chemisorption at 300 K as described elsewhere [2] was performed on each catalyst after an identical pretreatment, and the number of catalytic sites was taken to be the irreversible CO uptake.

2.2. Reaction kinetics measurements

Fig. 1 shows a schematic of the apparatus used to conduct reaction kinetics studies of the liquid-phase reforming of methanol and ethylene glycol. The reactor is a 6.3-mm od ($\frac{1}{4}$ inch) and 5-mm id stainless-steel tubular reactor consisting of a packed bed 3–10 mm long of sieved powder catalyst (0.1–0.3 g). A liquid solution of 10 wt% ethylene glycol or methanol in deionized water is introduced in an upflow configuration at 0.30 ml/min with an HPLC pump. The total pressure of the system is regulated to 22.4 or 29.3 bar with N_2 carrier gas, which bubbles through the effluent and sweeps gaseous products for analysis to gas chromatographs (GCs) equipped with thermal conductivity detectors (TCD). Hydrogen is separated via a Porapak Q column, carbon monoxide by a molecular sieve (5A) column, and CO_2 and alkanes by a Hayesep D column. Liquid products are collected in the gas-liquid separator and analyzed after each

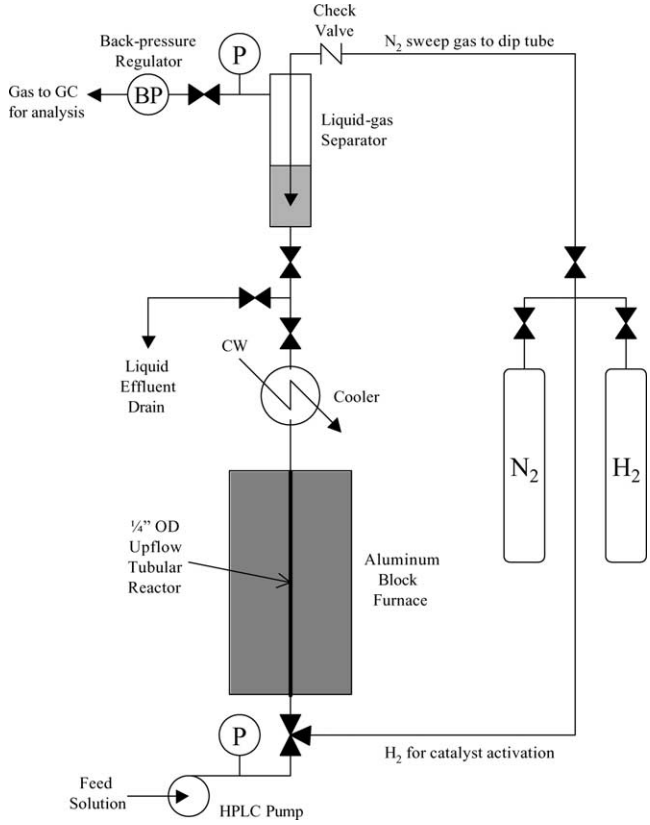

Fig. 1. Apparatus for reaction kinetics studies of liquid-phase oxygenate reforming.

run with a GC equipped with a flame-ionization detector (FID) and an Innowax column and an HPLC with an Aminex HPX 87H column and both refractive index (RI) and ultraviolet (UV) detectors. Reaction kinetics data were collected for up to 8 h on stream for each set of reaction conditions, to assure that the catalyst system reached steady state. Replicate runs with both methanol and ethylene glycol give a standard deviation in the hydrogen turnover frequency of 0.5 min^{-1} at 483 K and 0.2 min^{-1} at 498 K.

The furnace was a close-fitting, well-insulated aluminum block, heated externally with high-temperature heat tape. This construction allows for effective heat transfer to the reactor wall and provides isothermal operation of the reaction zone. The gas and liquid holdups in the system were minimized to reduce the time necessary for steady state to be reached and to decouple chemical phenomena in the reactor from the physical lag time in product sampling. A pressure gauge was fitted on the HPLC pump outlet to measure the pressure drop through the catalyst bed. Under reaction conditions, this pressure drop was less than 0.4 bar. The conversions of ethylene glycol and methanol were maintained below 3% to achieve differential reactor operation.

3. Transport limitations

The influence of transport phenomena on chemical kinetics measurements has been thoroughly analyzed from a theoretical point of view [3–11]. To supplement theoretical approaches, experimental tests have been developed to assess whether transport limitations are present. Koros and Nowak [12] proposed a method based on the fact that the reaction rate (μmol/(min g_{cat})) should be proportional to S, the number of active sites per unit volume of the reactor, in the absence of any transport limitations. In contrast, the reaction rate is proportional to $S^{1/2}$ when intraparticle mass transport is limiting, and the rate is related to S^0 when interphase mass transport limitations occur. Thus, if S is varied by diluting the active catalyst with an inert (maintaining particle size and geometry constant) and the rate is proportional to S, then the catalyst is operating in the kinetically controlled regime. This test probes both intraparticle and interphase limitations simultaneously without changing the flow field in the reactor.

Madon and Boudart [13] showed that the Koros-Nowak criterion could be applied to supported metal catalysts by varying the metal loading. Thus, in the kinetically controlled regime, the ratio of specific reaction rates is equal to the ratio of surface sites measured for two catalysts. The Madon–Boudart criterion is particularly useful because no inert diluent must be chosen, and pelletization no longer becomes an issue. Instead, catalyst preparation and pretreatment must be controlled to maintain the same metal dispersions for the catalysts, thus eliminating possible effects caused by structure-sensitive reactions.

4. Results

Dimensionless transport criteria for an aqueous environment were evaluated for the reactor system using several catalyst particle sizes. The highest temperature of the present study (i.e., 498 K) was selected and a high value of the catalyst pore tortuosity [14] (i.e., 10) was assumed to impose the most severe transport limitations encountered in the reactor-catalyst system. Table 1 shows computed values of dimensionless groups used to assess the importance of various transport limitations. Three cases are shown to illustrate the onset of transport limitations as the catalyst loading and particle size increase. Mass transfer becomes limiting before heat transfer, and interphase mass transfer becomes limiting only after intraphase mass transfer resistance is significant. For the largest particles with the highest metal loading, the internal effectiveness factor decreases to a value of about 0.8.

The presence of transport limitations for aqueous-phase reforming of 10 wt% ethylene glycol solutions was tested experimentally using the Madon–Boudart method. Accordingly, three Pt/Al_2O_3 catalysts with different metal loadings and similar Pt dispersions were prepared, and the rate of ethylene glycol reforming was measured on these catalysts at 483 and 498 K. The properties and performance of each catalyst are shown in Table 2. A plot of the rate of hydrogen production versus metal loading is shown in Fig. 2. The slope of this plot is approximately equal to unity for the 0.16 and 0.59 wt% Pt catalysts at 483 and 498 K, indicating that the Madon–Boudart test for the absence of transport limitations is satisfied in this regime. The slope of the line deviates from unity between catalyst loadings of 0.59 and 3.4 wt%. Some of this deviation may be caused by the lower dispersion of the high loading catalyst. However, transport limitations appear to be present for the high loading catalyst, since the slope decreases further from unity as the temperature is increased from 483 to 498 K.

Since transport limitations are absent for aqueous-phase reforming over 0.59 wt% Pt/Al_2O_3, this catalyst was selected for further studies of the intrinsic kinetics of methanol and ethylene glycol reforming. Fig. 3 shows the rates of hydrogen production at 498 K from ethylene glycol and methanol reforming versus the liquid-phase concentrations of these oxygenated hydrocarbons. The reaction order with respect to ethylene glycol concentration decreases from about 0.5 between 1 and 4 wt% ethylene glycol in the feed to about 0.3 between 4 and 10 wt% ethylene glycol in the feed. In contrast, the reaction order with respect to the liquid-phase methanol concentration is about 0.8 over the entire concentration range from 1 to 10 wt%. Since the selectivity to hydrogen is essentially 100%, the rate of CO_2 production can be determined by the reforming reaction stoichiometry.

Fig. 4 shows the effect of the system total pressure on the rates of methanol and ethylene glycol reforming at 483 K. It can be seen that the total pressure has a strong inhibiting effect on the rate of hydrogen production. As the total pressure of the system is lowered closer to the

Table 1
Computed transport criteria for the catalyst-reactor system in three configurations using the most severe reaction conditions

Catalyst:		3.43% Pt/Al_2O_3	3.43% Pt/Al_2O_3	0.59% Pt/Al_2O_3			
Particle treatment:		pelletized	−120/+230 mesh	−120/+230 mesh			
Max particle diameter (m):		0.0030	0.00013	0.00013			
Sites (μmol/g):		105	105	25			
	Formula		Computed values		**Target**	Criterion	Ref.
Internal effectiveness factor		0.78	0.99	1.00			
Interphase heat	$\frac{\lvert\Delta H\rvert r''' r_p^2}{hT_b}$	6.1×10^{-7}	4.6×10^{-11}	1.1×10^{-11}	$<6.2\times10^{-3}$	$0.15\frac{RT_b}{E}$	[6]
Interparticle heat	$\frac{\lvert\Delta H\rvert r''' r_p^2}{k_e T_w}$	7.5×10^{-9}	1.4×10^{-11}	3.0×10^{-12}	<0.015	$0.4\frac{RT_w/E}{[1+8(r_p/R_o)Bi_w]}$	[6]
Intraparticle heat	$\frac{\lvert\Delta H\rvert r''' r_p^2}{\lambda T_s}$	7.5×10^{-9}	1.3×10^{-11}	3.0×10^{-12}	<0.031	$\frac{0.75RT_s}{E}$	[3]
Isothermal pellet	$\lvert\gamma\beta\rvert$	2.7×10^{-3}	2.7×10^{-3}	2.7×10^{-3}	<0.025	$0.05n$	[7]
Isothermal pellet + film	$\left\lvert\gamma\beta+\frac{0.3n\gamma(-\Delta H)r_p r'''}{hT_b}\right\rvert$	2.8×10^{-3}	2.7×10^{-3}	2.7×10^{-3}	<0.025	$0.05n$	[7]
Intraparticle mass	$\frac{r''' r_p^2}{C_s D_e}$	6.7	0.012	2.9×10^{-3}	<3.5	3.5 for $n=0.5$	[10]
Interphase mass	$\frac{r''' r_p^2}{C_b k_c}$	0.41	1.4×10^{-4}	3.3×10^{-5}	<0.30	$0.15/n$	[4]
Length for axial dispersion (m)	$\frac{L}{2r_p}$	2.8×10^{-3}	2.8×10^{-3}	2.8×10^{-3}	<1.6	$\frac{10nD_{AB}}{r_p v}\ln(1-X)$	[7]
Intraparticle heat + mass	$\left\lvert\frac{nr''' r_p^2}{C_s D_e}-\frac{(-\Delta H)r''' r_p^2 E}{\lambda T_s RT_s}\right\rvert$	3.4	6.0×10^{-3}	1.0×10^{-3}	<1.0		[27]
Intraparticle + interphase heat + mass	$\frac{r''' r_p^2}{C_b D_e}$	13	0.023	4.9×10^{-3}	<2.0	$\frac{1+0.33\chi\gamma}{\lvert n-\gamma\beta\rvert(1+0.33n\omega)}$	[7]

Calculated transport criteria should be less than the values in bold to avoid limitations.

Table 2
Madon–Boudart test results for three Pt/Al_2O_3 catalysts sieved between 120- and 230-mesh size (63- to 125-μm sieve openings)

Catalyst	CO/Pt ratio	Carbon conversion to gas (%)		H_2 TOF (min^{-1})	
		483 K	498 K	483 K	498 K
0.16% Pt/Al_2O_3	0.63	0.2	0.4	4.3	9.4
0.59% Pt/Al_2O_3	0.82	1.0	1.9	4.2	9.0
3.43% Pt/Al_2O_3	0.60	1.6	3.4	3.5	7.0

bubble point of the feed solution (i.e., approximately equal to the vapor pressure of water plus the vapor pressure of the oxygenated hydrocarbon times its mole fraction), the rate becomes approximately minus third order in the total pressure. The effect of total pressure effect is less significant at pressures well above the bubble point.

A chemical explanation for the strong effect of the system total pressure on the rate of liquid-phase catalytic reforming can be formulated based on a pressure balance for the system. As presented in greater detail under Discussion, we suggest that the gaseous bubbles formed during liquid-phase reforming of methanol and ethylene glycol are composed of the reaction products plus the water and oxygenated hydrocarbon reactants at their respective vapor pressures. Since the total pressure of the bubbles is equal to the total pressure of the system, we may then calculate the hydrogen partial pressure in the catalyst bed. Fig. 5 shows a plot of the rate of hydrogen production from methanol and ethylene glycol reforming at 483 K versus the calculated hydrogen partial pressure. It can be seen that the rate of hydrogen production is inhibited by the hydrogen partial pressure, and

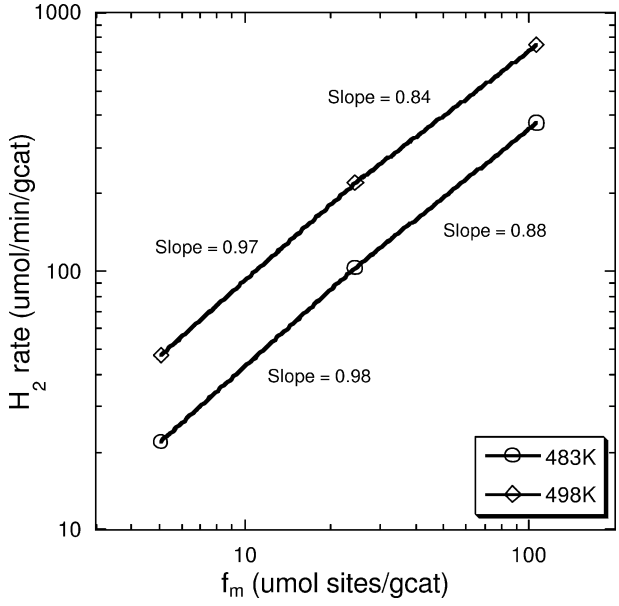

Fig. 2. A plot of the specific rate of hydrogen production as a function of the catalyst loading (10 wt% ethylene glycol feed solution at 483 and 498 K), showing that the Madon–Boudart criterion is satisfied for catalysts containing at least up to 0.59 wt% Pt and less than 3.4 wt% Pt. The total system pressure was maintained at 22.4 and 29.3 bar, respectively, approximately 3 bar above the vapor pressure of water at each temperature.

the reaction rate in approximately negative one-half order with respect to the hydrogen pressure for both methanol and ethylene glycol feedstocks.

The effect of temperature on the rate of reforming for methanol and ethylene glycol was studied while maintaining

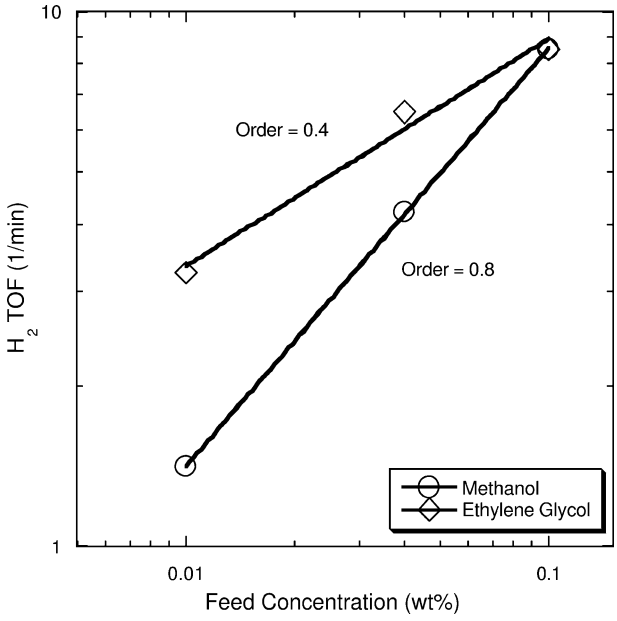

Fig. 3. The effect of methanol and ethylene glycol inlet concentration on the rate of hydrogen production over the range of 1–10 wt% in an aqueous feed solution. Experiments were conducted at 498 K and a total pressure of 29.3 bar.

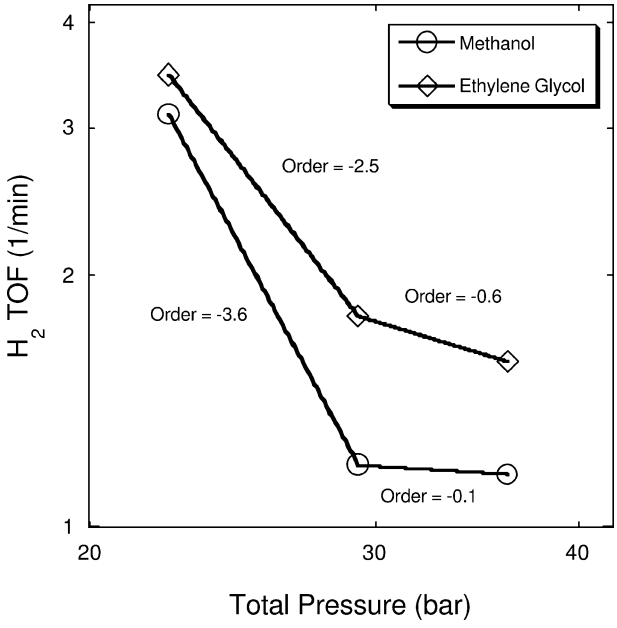

Fig. 4. The effect of total system pressure on the rate of hydrogen production. Experiments were conducted with a 10 wt% aqueous methanol or ethylene glycol feed solution at 483 K over a total pressure range of 22.4–36.2 bar.

the total pressure of the system at a value 3 bar above the vapor pressure of water at each temperature. In this way, the hydrogen partial pressure was maintained at a nearly constant value for each temperature. Accordingly, measurements of the rate of hydrogen production were made at 483 K and 22.4 bar total pressure, and at 498 K and 29.3 bar total pressure (corresponding to hydrogen partial

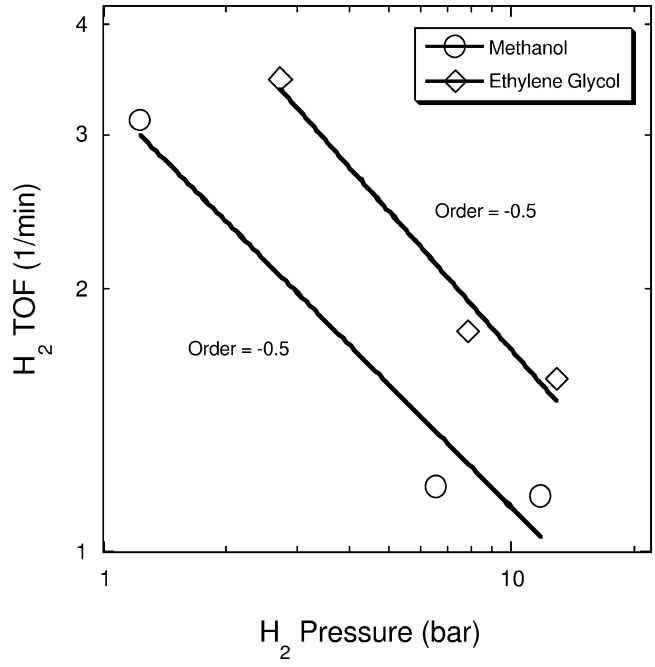

Fig. 5. The effect of hydrogen partial pressure on the rate of hydrogen production. Experiments were conducted with a 10 wt% aqueous methanol or ethylene glycol feed solution at 483 K over a total pressure range of 22.4–36.2 bar.

pressures of 1.5 and 3.0 bar for experiments with methanol and ethylene glycol, respectively). These measurements give apparent activation energy barriers of approximately 140 and 100 kJ/mol for methanol and ethylene glycol reforming, respectively.

Analysis showed that the liquid reactor effluent contained small amounts of by-products. Ethylene glycol effluents showed several alcohols, aldehydes, and acids. The liquid effluent from the highest conversion ethylene glycol run contained unreacted ethylene glycol, 170 wppm methanol, 110 wppm ethanol, 20 wppm glycolaldehyde, and less than 10 wppm each of glycolic acid, acetic acid, and acetaldehyde. Reaction kinetics runs with methanol in the feed showed only unreacted methanol. Traces of higher molecular weight condensation products were found in both methanol and ethylene glycol liquid reactor effluents. Although high-temperature water is known to be fairly corrosive, no dissolved Pt or Al (< 1 wppm) was detected in the reactor effluent by atomic absorption spectroscopy.

5. Discussion

The rate of the aqueous-phase ethylene glycol reforming reaction is fractional order with respect to the concentration of ethylene glycol in the feed, approaching low-order kinetics (i.e., 0.3) as the liquid-phase concentration approaches 10 wt%. These results suggest that the fractional surface coverage by adsorbed species derived from ethylene glycol is significant under the experimental conditions of the present

study. In contrast to ethylene glycol reforming, the methanol reforming reaction is nearly first order (i.e., 0.8) with respect to methanol over the liquid-phase concentration range from 1 to 10 wt%. The higher reaction order for methanol reforming may be due to the weaker adsorption of methanol on Pt surfaces compared to bidentate adsorbed ethylene glycol [15]. Thus, at high feed concentrations, the rates of reforming of methanol and ethylene glycol are similar, but the rate of methanol reforming is slower compared to ethylene glycol at lower feed concentrations, as seen in Fig. 3, due to weaker adsorption and thus lower surface coverages of adsorbed species derived from methanol.

An important aspect of the present study is that very low levels of CO (< 300 ppm) are detected in the gaseous effluents from aqueous-phase reforming of methanol and ethylene glycol over the alumina-supported Pt catalysts of this study. This observation suggests that the water–gas shift reaction may be an important aspect of the liquid-phase reforming process, as seen in steam reforming of methanol over supported Pt [16,17] and Ni [18] catalysts. In particular, it appears that reforming and water–gas shift reactions take place in the same reactor at the temperatures of the present study (e.g., at 500 K). The equilibrium constant, K_{WGS}, for the water gas shift reaction at 500 K is equal to 3100 bar, when the reaction is written in terms of liquid-phase water (i.e., $K_{\mathrm{WGS}} = P_{\mathrm{CO_2}} P_{\mathrm{H_2}} / P_{\mathrm{CO}} a_{\mathrm{H_2O}}$). For the dilute solutions of the present study, the activity of liquid water is essentially equal to unity. Thus, as the water–gas shift reaction becomes quasi-equilibrated, the corresponding ratio of pressures Q_{P} $(= P_{\mathrm{CO_2}} P_{\mathrm{H_2}} / P_{\mathrm{CO}})$ approaches the value of K_{WGS}. Reaction kinetics experiments conducted at higher conversions (e.g., 10–15%) where detectable amounts of CO can be observed indicate that the value of Q_{P} at 500 K is equal to 1100 bar, indicating that the water gas shift reaction is nearly equilibrated. Thus, it appears that the water–gas shift reaction may be responsible for providing a pathway for removing adsorbed CO from the Pt surface at the relatively low temperatures of this study, thereby preventing adsorbed CO from inhibiting reforming reactions by blocking surface sites. Without water present, carbon monoxide poisoning of metal surfaces has been well documented by TPD studies to occur at temperatures at near 500 K [19]. Infrared spectroscopic studies of the electrochemical oxidation of methanol [20] and ethylene glycol [21] show production of CO on Pt surfaces at low temperatures (e.g., 300 K), as confirmed by theoretical density functional calculations [22].

The results of the present study show that the rate of aqueous-phase reforming of methanol is similar to the rate of ethylene glycol reforming over Pt/alumina at temperatures near 500 K. This observation suggests that cleavage of the C–C bond in ethylene glycol is not a rate-limiting step in the reforming process, otherwise the rate of ethylene glycol reforming would have been slower than the rate of methanol reforming. Thus, it appears that aqueous-phase reforming reactions of methanol and ethylene glycol may be limited by the same surface processes, such as C–H and O–H bond cleavage steps leading to the formation of dehydrogenated surface intermediates, and steps involving the removal of adsorbed CO from the Pt surface by water–gas shift.

Since aqueous-phase reforming of methanol and ethylene glycol generates H_2, CO_2, and CH_4, (and smaller amounts of ethane), gas bubbles are formed within the liquid-phase flow reactor. These bubbles are not diluted by nitrogen carrier gas from the separator, because nitrogen is not soluble in the aqueous reactor effluent that stands between the catalyst bed and the separator. Accordingly, the total pressure inside the bubbles can be approximated as the total pressure of the system. Assuming vapor-liquid equilibrium, the bubbles should contain water and feed partial pressures commensurate with their vapor pressures in the feed solution. The remaining pressure must be the sum of the partial pressures of the product gases:

$$P_{\mathrm{system}} \approx P_{\mathrm{bubble}} = \sum_{\mathrm{feed}} P_i + \sum_{\mathrm{products}} P_j. \tag{7}$$

Since the relative concentrations of the product gases (i.e., the reaction selectivity) is known from analysis of the nitrogen-diluted stream ($P_{j,\mathrm{diluted}}$), the partial pressure of each product gas (P_j) in the bubbles can be found:

$$P_j = \frac{P_{j,\mathrm{diluted}}}{\sum_{\mathrm{products}} P_{j,\mathrm{diluted}}} \left(P_{\mathrm{bubble}} - \sum_{\mathrm{feed}} P_i \right). \tag{8}$$

Using this scheme to calculate the partial pressure of hydrogen in the reactor, we have found that the reaction order with respect to the hydrogen pressure is approximately -0.5. This inhibiting effect of hydrogen on the rate of reforming reactions could be caused by the blocking of surface sites by adsorbed hydrogen atoms. In addition, hydrogen could inhibit the rate by decreasing the surface concentrations of reactive intermediates formed from dehydrogenation of the oxygenated hydrocarbon reactants.

The effect of total pressure may also be caused in part by partial vaporization of the oxygenated hydrocarbon reactant, especially for the case of methanol reforming. Alternately, if the chemistry is dominated by liquid-phase reforming, changes in pressure may change the wetting efficiency of the catalyst. Catalyst wetting is of importance in gas–liquid–solid reactors [23], and system pressure affects the density and bubble size distribution of gases bubbling through the liquid [24,25].

It appears that alkane by-products formed during liquid-phase reforming are produced from the reactants by reaction pathways parallel to the production of hydrogen. For example, the formation of ethanol during liquid-phase reforming of ethylene glycol suggests that C–O bond cleavage in the ethylene glycol (i.e., dehydration) and subsequent hydrogenation have occurred. Similarly, methanol may be converted to methane. Cleavage of the C–O bond may take place by an acid-catalyzed pathway on the support or over the metal, while hydrogenation to form the alkyl group most

likely takes place over the metal surface. The alkane selectivity has also been shown to be relatively insensitive to conversion and to changes in hydrogen partial pressure caused by altering the total system pressures; therefore, it appears unlikely that alkanes are formed in significant amounts by series reactions involving H_2 and CO/CO_2 over the platinum-based catalysts of the present study; i.e., alkanes are not formed by methanation or Fischer–Tropsch reactions from CO/CO_2 and H_2.

We now speculate about the form of the rate expression for aqueous-phase reforming of an oxygenated hydrocarbon such as ethylene glycol. We suggest that the following reaction scheme may capture the essential surface chemistry:

$$C_2O_2H_6 + {}^* \overset{K_{EG}}{\rightleftarrows} C_2O_2H_6{}^* \quad \text{(quasi-equilibrated)},$$

$$H_2O + 2^* \overset{K_{H_2O}}{\rightleftarrows} OH^* + H^* \quad \text{(quasi-equilibrated)},$$

$$H_2 + 2^* \overset{K_{H_2}}{\rightleftarrows} 2H^* \quad \text{(quasi-equilibrated)},$$

$$CO_2 + {}^* \overset{K_{CO_2}}{\rightleftarrows} CO_2{}^* \quad \text{(quasi-equilibrated)},$$

$$C_2O_2H_6{}^* + {}^* \overset{k_{rxn}}{\rightarrow} C_2O_2H_5{}^* + H^*;$$

irreversible steps leading to $C_2O_2H_x{}^*$,

$$C_2O_2H_x{}^* + {}^* \overset{k_{C-C}}{\rightarrow} 2COH_y{}^*;$$

irreversible steps leading to CO^*,

$$CO* + OH^* \overset{k_{WGS}}{\rightarrow} CO_2{}^* + H^*;$$

where * represents a surface Pt site. We assume in this scheme that adsorption steps involving ethylene glycol, water, H_2, and CO_2 are quasi-equilibrated. We also assume that reforming takes place through a series of irreversible steps, since the equilibrium constants for these steps are probably rather large in view of the very favorable thermodynamics for the overall reforming reaction leading to H_2 and CO_2. These reforming reactions involve dehydrogenation of adsorbed ethylene glycol to form adsorbed $C_2O_2H_x{}^*$ species (rate constant k_{rxn}), cleavage of the C–C bond to form adsorbed $COH_y{}^*$ species (rate constant k_{C-C}), further dehydrogenation leading to adsorbed CO^*, and removal of adsorbed CO^* by the water–gas shift reaction (rate constant k_{WGS}). We have assumed that CO_2 is formed from CO by the water–gas shift reaction; however, we note it is also possible that reforming forms CO_2 by reaction of water or hydroxyl groups with more hydrogenated surface intermediates (i.e., the reaction scheme does not pass through adsorbed CO^*). This development is similar to the vapor phase decomposition of methanol over Pt/SiO_2 and other catalysts [26]. If we now assume that the most abundant surface species are adsorbed $C_2O_2H_6{}^*$, H^*, OH^*, and CO^*, then the following rate expression for aqueous-phase reforming of ethylene glycol is obtained:

$$r = k_{rxn}K_{EG}P_{EG} \Big/ \left[1 + \sqrt{K_{H_2}P_{H_2}}\left(1 + \frac{k_{rxn}K_{EG}P_{EG}}{k_{WGS}K_{H_2O}P_{H_2O}}\right) + K_{EG}P_{EG} + \frac{K_{H_2O}P_{H_2O}}{\sqrt{K_{H_2}P_{H_2}}}\right]^2. \quad (9)$$

The terms in the denominator of this rate expression correspond (from left to right) to surface coverage by vacant sites, H^*, CO^*, $C_2O_6H_6{}^*$, and OH^*. This rate expression is consistent with the observed negative reaction order with respect to hydrogen, and this negative order is explained by the blocking of surface sites by adsorbed H^* or CO^*. In addition, the rate expression is consistent with the observed fractional reaction order with respect to ethylene glycol, and this fractional order is explained by the blocking of surface sites by adsorbed $C_2O_2H_6{}^*$ or CO^*.

Aqueous-phase reforming of methanol may take place by a reaction scheme similar to that described above for ethylene glycol, without the step involving cleavage of the C–C bond. The negative reaction order with respect to hydrogen can be explained by the blocking of surface sites by adsorbed H^* or CO^*. The nearly first-order reaction kinetics with respect to methanol can be explained by noting results from DFT calculations which show that molecular adsorption of methanol on Pt is weaker compared to molecular adsorption of ethylene glycol [15]. We also note that the observed reaction kinetics for aqueous-phase reforming of methanol may be complicated by the possible contribution of vapor-phase methanol reforming, since methanol is more volatile compared to ethylene glycol.

6. Conclusions

Reaction kinetics measurements on Pt/Al_2O_3 catalysts with different metal loadings were carried out (employing the Madon–Boudart test) to determine kinetically controlled rates for aqueous-phase reforming of methanol and ethylene glycol at 483 and 498 K. These results show that methanol and ethylene glycol have similar reactivity for aqueous-phase reforming over Pt/Al_2O_3 at consistent C/H_2O feed ratios, indicating that C–C bond cleavage is not rate limiting for ethylene glycol reforming. The rate of hydrogen production is higher order in methanol (0.8) than ethylene glycol (0.3–0.5), while the reaction is weakly inhibited by hydrogen for both feedstocks (-0.5 order). Thus, it appears that the surface coverage by species derived from ethylene glycol is higher than from methanol under aqueous-phase reforming reaction conditions. The inhibiting effect of hydrogen on the rate of reforming could be caused by the blocking of surface sites by adsorbed hydrogen atoms. In addition, hydrogen could inhibit the rate by decreasing the surface concentrations of reactive intermediates formed from dehydrogenation of the oxygenated hydrocarbon reactants. The rate of aqueous-phase reforming is more temperature dependent for methanol than ethylene glycol, with apparent activation bar-

riers of 140 and 100 kJ/mol, respectively, from 483 K and 22.4 bar total pressure to 498 K and 29.3 bar total pressure.

The liquid-phase environment of the present study favors the water–gas shift reaction, thereby mitigating the potential blocking of surface sites by adsorbed CO species. Accordingly, low levels of CO (< 300 ppm) are detected in the gaseous effluents from aqueous-phase reforming of methanol and ethylene glycol over alumina-supported Pt catalysts, and aqueous-phase reforming of both oxygenated hydrocarbons over Pt/Al_2O_3 leads to nearly 100% selectivity for the formation of H_2 (compared to the formation of alkanes). Since the selectivity for hydrogen production is essentially independent of conversion, it appears that the series hydrogenation of CO/CO_2 to alkanes is not significant over Pt/Al_2O_3 under the conditions of the present study.

Inhibition of the reaction rate by increased system pressure is caused by a corresponding increase in the partial pressure of hydrogen in the reactor. In addition, the effect of total pressure on the reaction rate may be caused by physical phenomena such as gas–liquid holdup and catalyst wetting. The observed reaction kinetics of this study for ethylene glycol reforming can be explained by a reaction scheme involving quasi-equilibrated adsorption of ethylene glycol, water, H_2, and CO_2, combined with irreversible steps involving dehydrogenation of adsorbed ethylene glycol to form adsorbed $C_2O_2H_x{}^*$ species, cleavage of the C–C bond to form adsorbed $COH_y{}^*$ species, further dehydrogenation leading to adsorbed CO*, and removal of adsorbed CO* by water–gas shift. Aqueous-phase reforming of methanol may take place by a reaction scheme, without the step involving cleavage of the C–C bond. The nearly first-order reaction kinetics with respect to methanol can be explained by weaker adsorption of methanol compared to molecular adsorption of ethylene glycol. The observed reaction kinetics for aqueous-phase reforming of methanol may also be complicated by the possible contribution of vapor-phase methanol reforming.

Acknowledgments

This work was supported by US Department of Energy (DOE), Office of Basic Energy Sciences, Chemical Sciences Division. We also acknowledge funding from the Energy Center of Wisconsin and the University of Wisconsin Office of University-Industrial Relations. We thank David Wishnik and Bret Wagner for assistance in collecting reaction kinetics data.

Appendix A. Nomenclature

C_b	Bulk-phase reactant concentration
C_p	Heat capacity at constant pressure
C_s	Concentration of reactant at the external surface of the catalyst particle
D_{AB}	Bulk binary diffusivity of species A in species B
D_e	Effective diffusivity
E	Activation energy of the reaction
h	Heat transfer coefficient
ΔH	Heat of reaction
k_c	Mass–transfer coefficient between the catalyst and bulk phases
k	Thermal conductivity of liquid
k_e	Effective thermal conductivity across the catalyst bed
K	Equilibrium constant
L	Catalyst bed length
n	Reaction order
P	Pressure
Q	Reaction quotient
R	Gas constant
R_o	Outer radius of reactor
R_b	radius of catalyst bed
r'''	Reaction rate per catalyst volume
r_p	Catalyst particle radius
S	Active sites per catalyst bed volume
T_b	Temperature of the bulk phase
T_s	Catalyst surface temperature
T_w	Reactor wall temperature
$\bar{v}$	Superficial velocity
X	Dimensionless conversion
β	$(-\Delta H)D_eC_s/(\lambda T_s)$
γ	$E/(RT_s)$
ε	Pore volume fraction of the catalyst pellet
χ	$\lvert-\Delta H\rvert r_p r'''/(hT_b)$
λ	Thermal conductivity of the catalyst particle
μ	Static viscosity
ρ	Density
τ	Tortuosity factor
ω	$r_p r'''/(C_b k_c)$

References

[1] R.D. Cortright, R.R. Davda, J.A. Dumesic, Nature 418 (2002) 64.
[2] R.R. Davda, J.W. Shabaker, G.W. Huber, R.D. Cortright, J.A. Dumesic, submitted for publication.
[3] J.B. Anderson, Kagaku Kogaku (Chem. Eng. Jpn.) 147 (1962) 191.
[4] J.J. Carberry, AICHE J. 7 (1961) 350.
[5] G.F. Froment, K.B. Bischoff, Chemical Reactor Analysis and Design, Wiley, New York, 1990.
[6] D.E. Mears, J. Catal. 20 (1971) 127.
[7] D.E. Mears, Ind. Eng. Chem. Proc. Des. Dev. 10 (1971) 541.
[8] C.N. Satterfield, Mass Transfer in Heterogeneous Catalysis, MIT Press, Cambridge, MA, 1970.
[9] J.M. Smith, J. Chem. Eng. Japan 6 (1973) 191.
[10] P.B. Weisz, C.D. Prater, Adv. Catal. 6 (1957) 143.
[11] P.B. Weisz, Z. Phys. Chem. 11 (1954) 1.
[12] R.M. Koros, E.J. Nowak, Chem. Eng. Sci. 22 (1967) 470.
[13] R.J. Madon, M. Boudart, Ind. Eng. Chem. Fundam. 21 (1982) 438.
[14] C.G. Hill Jr., An Introduction to Chemical Engineering Kinetics & Reactor Design, Wiley, New York, 1977.

[15] R.R. Davda, R. Alcala, J.W. Shabaker, G. Huber, R.D. Cortright, M. Mavrikakis, J.A. Dumesic, in: Fourth Tokyo Conference on Advanced Catalytic Science and Technology, Tokyo, Japan, 2002.
[16] K.T.N. Takahashi, H. Kobayashi, Chem. Lett. 4 (1985) 759.
[17] N. Takezawa, N. Iwasa, Catal. Today 36 (1997) 45.
[18] K. Mizuno, Y. Yokohama, N. Wakejima, Y. Takeuchi, A. Watanabe, Chem. Lett. 5 (1986) 1969.
[19] J. Novakova, L. Kubelkova, Appl. Catal. B 14 (3–4) (1997) 273.
[20] Y. Zhu, H. Uchida, T. Yajima, M. Watanabe, Langmuir 17 (2001) 146.
[21] J.F.E. Gootzen, W. Visscher, J.A.R. van Ween, Langmuir 12 (1996) 5076.
[22] S.N.M. Desai, K. Kourtakis, J. Phys. Chem. B 106 (2002) 2559.
[23] M.P. Dudukovic, F. Larachi, P.L. Mills, Chem. Eng. Sci. 54 (1999) 1975.
[24] I. Iliuta, J. Chem. Tech. Biotechnol. 68 (1997) 47.
[25] I. Iliuta, F.C. Thyrion, Chem. Eng. Sci. 52 (1997) 4045.
[26] S.H.T. Imamura, Y. Saito, H. Aritani, H. Kanai, Y. Matsumura, N. Tsuda, Catal. Today 50 (1999) 369.
[27] H. Kubota, Y. Yamanaka, I.G.D. Lana, J. Chem. Eng. Jpn. 2 (1969) 71.